Available online at www.sciencedirect.com
ScienceDirect
International Journal of Thermal Sciences 48 (2009) 488–501
International Journal of Thermal Sciences
www.elsevier.com/locate/ijts

Experimental study of laminar flames obtained by the homogenization of three forest fuels

Virginie Tihay [a,*], Albert Simeoni [a], Paul-Antoine Santoni [a], Lucile Rossi [a], Jean-Pierre Garo [b], Jean-Pierre Vantelon [b]

[a] *SPE – UMR 6134 CNRS, University of Corsica, Campus Grossetti, BP 52, 20250 Corte, France*
[b] *LCD – UPR 9028 CNRS, ENSMA, University of Poitiers, 1 avenue Clément Ader, Téléport 2, BP 40109, 86961 Futuroscope Chasseneuil Cedex, France*

Received 30 May 2007; received in revised form 19 March 2008; accepted 21 March 2008

Available online 24 April 2008

Abstract

This work aims to improve the understanding of the parameters involved in the burning of vegetative fuels. As the role of the surface-to-volume ratio is already known, we focused on the influence of other parameters. Three Mediterranean species (*Pinus pinaster*, *Erica arborea* and *Cistus monspeliensis*) were crushed in order to decrease the surface-to-volume ratio effects. The burning of these fuel samples produces unsteady, axisymmetric, non-premixed, laminar flames. The thermal properties and the mass loss of the crushed fuels, the distribution of temperature inside the sample and in the flame, the gases released by the fuels and the flame geometry were investigated. Thanks to these experimental data, the influence of the different fuel properties was underlined. We observed that the mass burning rate of the samples mainly controls the flame dynamics. However, the combustion kinetics in the flame depends on the degradation gases released by the fuels: the reaction zone is shifted and the flame height is changed. It appears that the composition of the degradation gases has to be taken into account to improve forest fire modeling.

Keywords: Laminar flame; Forest fuels; Degradation gases; Coupling gas–solid

1. Introduction

Fires devastate regularly forests and scrublands as well as populated areas all over the world. Foresters and fire fighters are faced with problems such as the management of wildland/urban interfaces and safety zones. To deal with this kind of situations, the fire phenomenon and specially the combustion of vegetation need to be better understood. Although the experiments at field scale are valuable to validate the numerical models of fire spread, they are not suitable to study precisely the influence of each fuel property on the combustion. Experiments at laboratory scale allow focusing on accurate phenomena as the fire parameters are monitored and controlled. Among the experiments conducted at laboratory scale to investigate the burning of vegetative fuels, the following kinds of studies were carried out:

- Thermal analysis and calorimetric studies [1–5] investigate the thermal degradation processes of the plant species. They provide information about the combustion kinetics and its heat release. The heating rate is generally less than 40 K min^{-1}. Thus, the experimental conditions are far from actual wildfires.
- Static combustion experiments are dedicated to the burning of forest fuel. Samples are introduced in cylindrical baskets [6,7]. The mass loss, the flame geometry and the temperature distribution are analyzed.
- Different sets of fire propagation in pine needle beds are carried out by a lot of authors [8–14]. These experiments are mainly focused on the determination of the rate of spread under different conditions (wind, slope, fuel characteristics…) and are used to validate numerical models.
- The last aspect concerns the degradation gases released by forest fuels. Since the pioneering work of Grishin [15], the combustible part of the devolatilization products is consid-

* Corresponding author. Tel.: +(33) 495 450 121; fax: +(33) 495 450 162.
E-mail address: tihay@univ-corse.fr (V. Tihay).

1290-0729/$ – see front matter
doi:10.1016/j.ijthermalsci.2008.03.018

Nomenclature

h	enthalpy	J
HF	heat flow	W
Δh_a	heating value per mass of air	$kJ\,kg^{-1}$
L	length	m
m	mass	kg
Δh	reaction enthalpy	$kJ\,kg^{-1}$
C_p	specific heat capacity	$J\,kg^{-1}\,K^{-1}$
f_s	stoechiometric coefficient in air	
T	temperature	K
t	time	s
V	volume	m^3
v	value of the RGB components	
a	thermal diffusivity ($\lambda/\rho C_p$)	$m^2\,s^{-1}$
l	width	m

Greek symbols

ρ_{bulk}	bulk density	$kg\,m^{-3}$
α	fuel packing ratio	
β	heating rate	$K\,s^{-1}$
ρ	mass density	$kg\,m^{-3}$
τ	standard deviation	
σ	surface-to-volume ratio	m^{-1}
λ	thermal conductivity	$W\,m^{-1}\,K^{-1}$

Subscripts

B	blue
empty	empty pan
ethanol	ethanol
G	green
mean	mean value
P	constant pressure
reference	pan with reference sample
sample	pan with sample
R	red
k	time increment

ered to be carbon monoxide burning in air, whatever the vegetative species. However, these fuels are complex materials and the mixture composition of their degradation gases depends on the vegetative species [5].

According to these works, the prevailing property, which influences the combustion of vegetative fuels is the surface-to-volume ratio. However, there is no study which points out the influence of the other fuel properties and in particular of the degradation gases. Thus, one can wonder whether (and how) other parameters are involved. In order to answer to this question, three different species (*Pinus pinaster*, *Erica arborea* and *Cistus monspeliensis*) were crushed and sieved to decrease the influence of the surface-to-volume ratio, which hides the contribution of the other fuel properties. We studied experimentally unsteady, axisymmetric, non-premixed laminar flames resulting from the burning of the samples. These flames bring three main advantages. Firstly, they ensure a good reproducibility of the experiments. Secondly, they allow pointing out the combustion kinetics in the flames, which is often hidden by the turbulence. Finally, time-varying laminar diffusion flame is a class of non-premixed combustion [16] bridging the gap between steady laminar combustion and turbulent combustion that is encountered in forest fires. It is clear that the results obtained with laminar flames cannot be directly extended to real vegetation. However, this work can help to explain the combustion processes occurring in a larger scale more realistic turbulent flames. The study was conducted in two steps. On one hand, the thermal properties of the crushed samples were obtained. A differential scanning calorimeter (DSC) and a hot disk technique were used for the determination of specific heat and thermal conductivity, respectively. The gases released by the degradation of the fuels were determined with a tube furnace connected to a gas chromatograph and a hygrometer. On the other hand, the temperature distribution both in flame and inside the crushed samples, the flame height and the flame radius as well as the mass loss were measured. The experimental procedures are described in the following section. Next, global observations are provided for the burning of a sample. The behavior of the crushed fuel is then investigated and the gas phase is characterized. Finally, the coupling between the fuel sample and the flame is discussed.

2. Experimental devices and methods

2.1. Fuel samples

We studied the burning of three Mediterranean fuels: *Pinus pinaster*, *Erica arborea* and *Cistus monspeliensis* involved in wildland fires. These plants belong to the tree stratum, to the higher shrub layer and to the lower shrub layer, respectively. The needles of *Pinus pinaster* and the leaves and twigs of *Erica arborea* and *Cistus monspeliensis* were collected in winter during a period of hydrous stress for vegetation. Before experiments, they were oven-dried at 60 °C during 24 hours. Then, they were crushed and sieved to a particle size of 0.6–0.8 mm to ensure similar geometrical parameters for the three species. The moisture content due to self-rehydration was less than 2% for all samples before each repetition.

2.2. Time-varying, axisymmetric, diffusion flame

2.2.1. Experimental device

The experimental device is shown in Fig. 1. The fuel samples were in the shape of a cylinder with a diameter of 3.5 cm and a mass of 1.5 g. The depth of the sample depended on the bulk densities of the fuel (ranging from 4 to 5 mm). The combustion set-up was composed of a one square meter plate drilled at its centre. A ten square centimetres insulator was

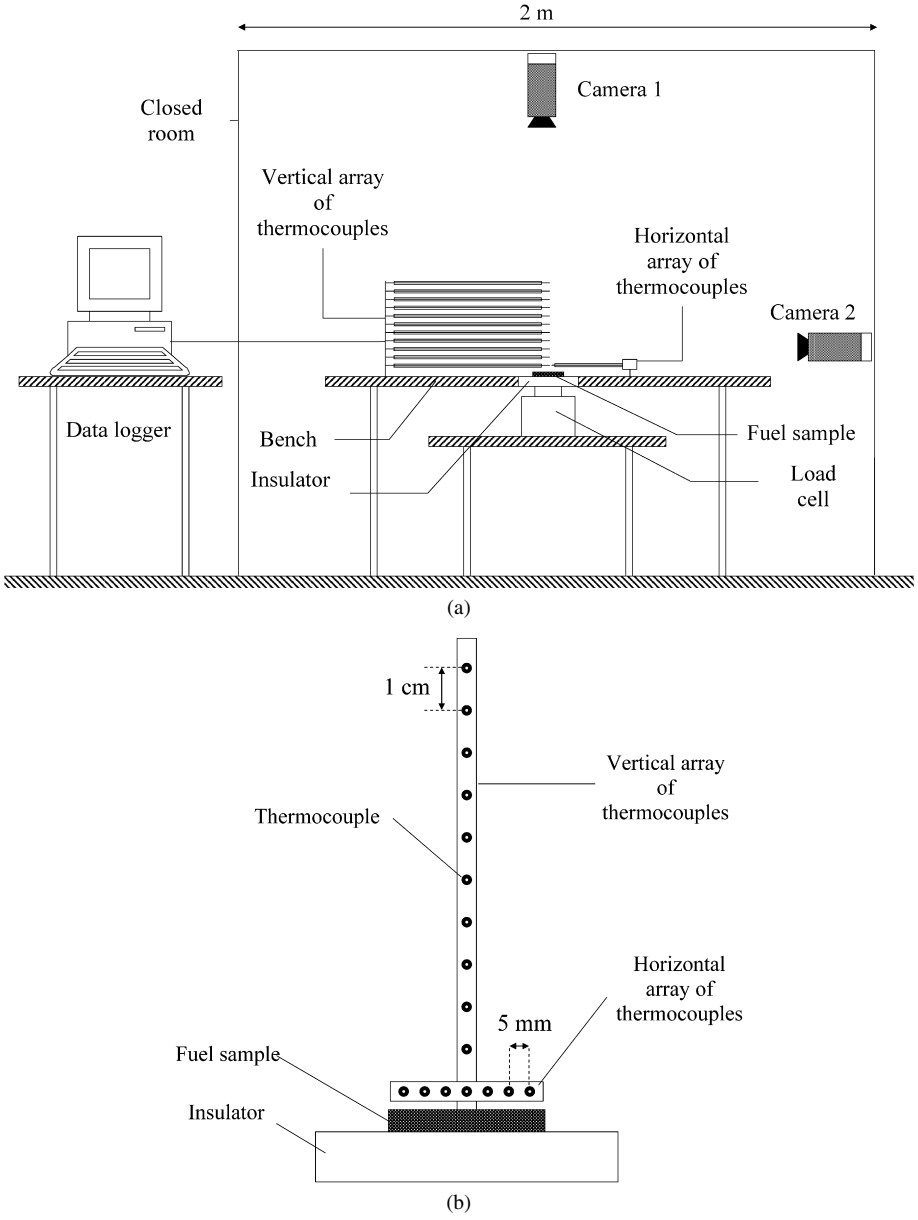

Fig. 1. Sketch of the experimental apparatus. (a) Global view. (b) Side view.

included at this location to support the fuel samples. It was positioned on a load cell in order to measure the fuel mass loss as a function of time. To insure a fast and homogeneous ignition, a small amount of ethanol (0.7 mL) was spread uniformly on the sample and was ignited with a flame torch. An array of 11 thermocouples was positioned above the crushed fuel along the flame axis. The first thermocouple was placed 1 cm above the top of the support and the others were located 1 cm from each other. A second array of thermocouples was located horizontally movable at different heights to obtain the temperature along the flame radius and inside the crushed sample. The spacing between these thermocouples was 5 mm. The thermocouples used were mineral-insulated integrally metal-sheathed pre-welded type K (chromel–alumel) pairs of wire with an exposed junction. At the exposed junctions, the wires are 50 μm in diameter. The load cell was chosen for its short response time (0.2 s) compared to the analytical balances which have a response time greater than 3 s. The uncertainty in temperature and mass measurements were respectively 0.5 °C and 0.031 g. The sampling frequency was 100 Hz. Two visible cameras were located inside the room (Fig. 1). Camera 1 followed the flame behavior and the flame height. Camera 2 was placed above the flame in order to record the regression of the flame basis. The ambient temperature was 21 °C and the relative humidity was 50%. At least five repetitions were made to collect reliable data for each fuel.

2.2.2. *Image processing*

The experiments were recorded on DV-PAL tape (images capture frequency: 1/25 s, image size: 720 × 576). The films were then exported on a computer in an AVI standard. Before the first experiment, a short video of a ruler put at the flame

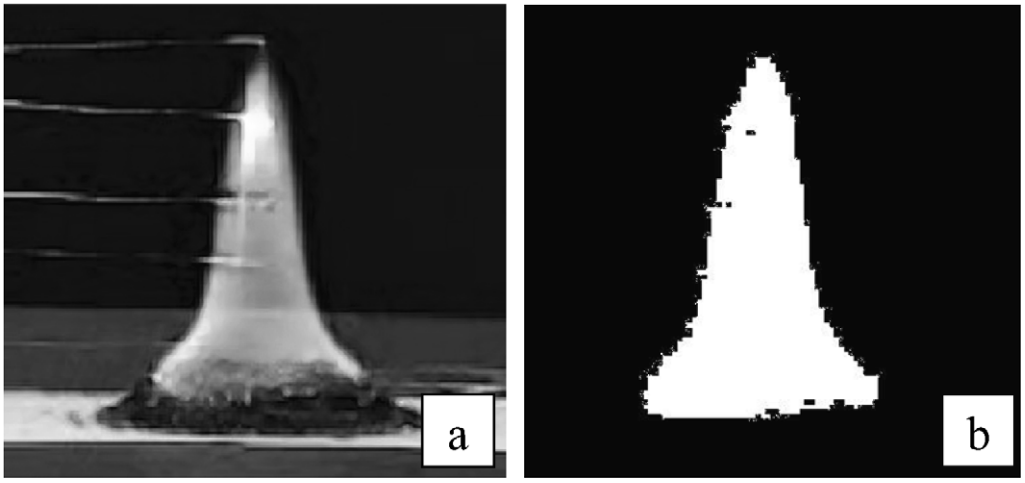

Fig. 2. Image processing. (a) Image extracted from the movie. (b) Binary image.

position was carried out in order to obtain a geometrical reference of measurement. An image processing procedure was developed in order to follow the flame height and the flame radius (recorded by camera 1 and 2 in Fig. 1) as a function of time during combustion. Images were extracted from videos with a sampling rate of 0.5 Hz as the flame was laminar, axisymmetric and did not flicker (Fig. 2(a)). This frequency allowed reducing the processing time without loosing accuracy. Next, a flame region segmentation procedure using RGB color space was applied on each image; more precisely on a square image zone containing the flame. This restriction allowed eliminating spurious detection like the presence of thermocouples. On the first extracted image, a set of pixels from the flame region were used as a reference. The "average" and the standard deviation of their RGB components were computed [17]. Then, each pixel was associated to a RGB vector $\vec{v} = (v_R, v_G, v_B)$. The denomination "mean" is relative to the average color of the reference zone. The measurement of similarity was carried out by using the Euclidean distance. An arbitrary point in RGB color space is similar to the flame zone if the distance between their RGB vectors is less than a specific threshold equal to 25 (higher values provided the same results):

$$D(\vec{v}, \vec{v}_{\text{mean}}) = \sqrt{(v_R - v_{\text{mean},R})^2 + (v_G - v_{\text{mean},G})^2 + (v_B - v_{\text{mean},B})^2} < 25 \quad (1)$$

Color-related information was then replaced by binary data. The pixels belonging to the flame were colored in white and the others in black (Fig. 2(b)). Next, the flame height and the flame radius were computing using Cartesian coordinates of the white area in the image plane. For the frontal view, the flame height corresponded to the height of the white area. In the case of top vision, the flame radius was the average diameter of the white area.

2.3. Geometrical properties of the samples

2.3.1. Bulk density

For determining the bulk densities ρ_{bulk} of the samples, a fixed volume was filled with fuel and weighted. These measurements were repeated ten times. An average of these values was calculated as well as the standard deviation.

2.3.2. Surface-to-volume ratio

The mean surface-to-volume ratio σ of the particles was obtained with a granulometric analysis. A sample of each species was treated by image processing using a high resolution scanner. It provided the mean length and the width of the particles. By assuming that the shape of the particles was a cylinder, the mean surface-to-volume ratios were calculated for each sample with the following relation:

$$\sigma = \frac{2}{L} + \frac{4}{l} \quad (2)$$

2.4. Physical properties of the samples

2.4.1. Specific heat

The measurements of the specific heat were performed using a differential scanning calorimeter (model DSC Setaram® 131). It is a thermal analysis technique in which the difference in the amount of heat required to increase the temperature of a sample and a reference are measured as functions of temperature. The samples were about 50 mg and were placed in an aluminium pan. The experiments were carried out at atmospheric pressure under air flow. In order to determine the specific heat of the samples, a "three-step" method with two pans was used: the same temperature program was applied to each sample, to a reference sample (i.e. zinc) and to an empty pan. The temperature program is based on a stepwise method. Each run consists in successive temperature increments of 20 °C performed at 5 °C min^{-1}. After each increment, a waiting period of 5 min is observed to obtain a stable signal. The temperatures ranged from 80 to 200 °C what allowed studying the fuel sample just

before its thermal degradation. Mean specific heat in the range of temperature $[T_k, T_{k+1}]$ was calculated with the following relationship:

$$C_{p_{\text{mean,sample}}}(T_k \to T_{k+1}) = C_{p_{\text{mean,reference}}} \frac{m_{\text{reference}}}{m_{\text{sample}}} \times \frac{\int_{T_k}^{T_{k+1}} HF_{\text{sample}}\, dT - \int_{T_k}^{T_{k+1}} HF_{\text{empty}}\, dT}{\int_{T_k}^{T_{k+1}} HF_{\text{reference}}\, dT - \int_{T_k}^{T_{k+1}} HF_{\text{empty}}\, dT} \quad (3)$$

where HF stands for the heat flow, m is the mass of the sample, C_p represents the specific heat and k is a time. The details concerning Eq. (3) are provided in Appendix A.

2.4.2. Thermal conductivity

Thermal conductivity measurements were conducted using the hot disk technique [18], which is a transient plane source method. The hot disk technique can be used to measure thermal conductivity in the range of 0.005 to 500 $\mathrm{W\,m^{-1}\,K^{-1}}$. The hot disk sensor is made of a double spiral of nickel wire. During the experiments, the hot disk sensor was placed in the fuel sample. A small constant current was supplied to the sensor used as a temperature monitor. The temperature increase in the sensor was accurately determined through resistance measurement. By monitoring this temperature increase over a short period of time after the beginning of the experiment, it is possible to obtain accurate information on the thermal conductivity of the fuel sample. The thermal conductivity measurements were performed for the three species and for two temperatures: 100 and 200 °C. The uncertainty of the measurements is 5%.

2.4.3. Density and fuel packing ratio

For each sample, the density measurement was performed with a graduated test tube of 10 ml. The determination of the density was carried out in three steps. Firstly, a mass of sample (m_{sample}) was placed in the tube test. 3 ml of absolute ethanol (V_{ethanol}) was added in the tube. The absolute ethanol allows obtaining the same results as water. However, it ensures the total immersion of the fuel sample in the fluid and has a highest wetting power. Finally, the total volume (V_{total}) was noted. The density of the sample is given by:

$$\rho_{\text{sample}} = \frac{m_{\text{sample}}}{V_{\text{total}} - V_{\text{ethanol}}} \quad (4)$$

These measurements were repeated three times. The fuel packing ratio corresponds to the ratio between the bulk density and the density of the fuels. It is given by the relation:

$$\alpha = \frac{\rho_{\text{bulk}}}{\rho_{\text{sample}}} \quad (5)$$

2.5. Composition of the pyrolysis gases

The tube furnace apparatus used as pyrolyser is shown in Fig. 3. It is made of a cylindrical furnace 43.5 cm long with an internal diameter of 6.5 cm. The reactor inside, is 86 cm long with an inner diameter of 5 cm. Two thermocouples were used to record the temperature history in the furnace. One was

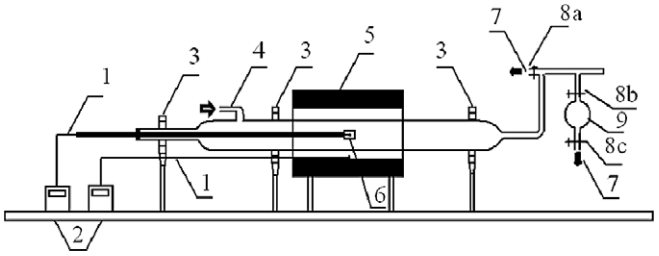

Fig. 3. Schematic of the tube furnace (1 thermocouple, 2 temperature controller, 3 bearing, 4 nitrogen injection, 5 electric furnace, 6 sample box, 7 air suction, 8a–c valves, 9 gas samplers).

fixed on the inner surface of the furnace and the other was placed in the combustion chamber to follow the temperature in the sample at different height. Experiments were conducted for the three fuels. Thermogravimetric analysis showed that vegetative samples lose about 60% of their mass between 280 and 430 °C [19]. Thus, we present only the gas mixtures released during this range of temperature as they are characteristic of the combustion in the flame. The temperature of the furnace was set at 450 °C. This furnace temperature allows the samples attaining the chosen range of temperature. Gases were collected into a balloon called the gas sampler, hereafter. The sample box filled with 4 g of sample was kept outside of the furnace until the temperature of the furnace reached the required value. At the same time, air suction was switched on, the gas sampler was opened and nitrogen was injected at 1 L/min to obtain an inert atmosphere in the device. Once the temperature was stable, the sample was introduced inside the furnace. The injection of nitrogen was stopped, gas sampler was closed and the valve (8a on Fig. 3) allowing the ejection of gases outside the apparatus was opened. When samples reached the required temperature, gas sampling began. Valve 8a was closed, a gas sampler was opened and nitrogen was injected into the reactor to fill the gas sampler with pyrolysis gases. Then the gas sampler was directly attached either to the gas chromatograph (Flame Ionization Detector and Thermal Conductivity Detector) or to the hygrometer (EdgeTech Model 2001 Series DewPrime) measuring the dew point with a resolution of 0.1 °C. The mass loss of the sample between 280 and 425 °C was measured for each test. At least three repetitions were carried out. Three tests without fuel were also carried out to verify that there was no leak.

3. Results and discussion

The main objective of this section is to determine the driving parameters of the fuel combustion. To proceed, we compare the flames resulting from the burning of the three crushed vegetative fuels (*Pinus pinaster*, *Erica arborea* and *Cistus monspeliensis*). First of all, we describe the global behavior of the three flames. Next, the physical and geometrical properties of the crushed fuel are depicted as well as the temperature in the sample and its mass loss. Then, the composition of the degradation gases and the temperature distribution in the flame are presented. Finally, the coupling between the sample and the

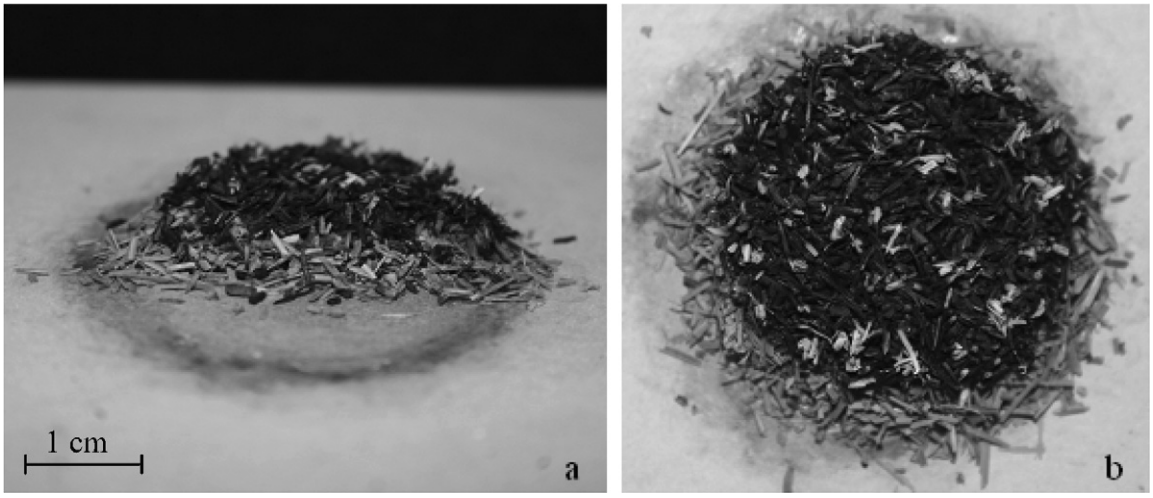

Fig. 4. The remaining solid phase after extinction for *Pinus pinaster*. (a) Cut-away view, (b) top view.

flame is underlined through the study of the flame geometry and the axial temperature.

3.1. Burning experiments

The same global tendency was observed for the burning of all the vegetative fuels, including three different stages: ignition, laminar flame and extinction. The first stage lasted about 60 s and corresponded to a flickering flame. Then, the flame became laminar. It was axisymmetric and slightly conical with a narrow tip (Fig. 2). The flame height and radius decreased slowly. To explain the visually observed transition from a flickering to a laminar flame, frequency domain analyses of temperature profiles were performed. Between 0 and 60 s, the graph showed an 8 Hz predominant frequency characteristic of ethanol. The flame fluctuations were due to the presence of the ethanol used to ignite the sample. After 60 s, the 8 Hz frequency vanished on the frequency domain analyses as the ethanol was completely burned. The fuel was only composed of the degradation gases and the flame became laminar. Finally, the last stage concerned the flame extinction. The remaining solid phase was essentially made up of carbon at the surface of the sample with a certain amount of unburned fuel near the support (Fig. 4). Contrary to the other samples, the particles of *Erica arborea* were covered by tar. For the whole species, a small and negligible amount of ashes was observed at the surface. The combustion time depended on the species. It lasted on average 100, 155 and 170 s, respectively, for *Cistus monspeliensis, Pinus pinaster* and *Erica arborea*.

3.2. Description of the crushed sample

3.2.1. Ultimate analysis

The ultimate analysis of each fuel is presented in Table 1. The composition in C, H, and O of the samples is close. The main differences concern the ash contents. *Cistus monspeliensis*'one is nine times greater than for *Pinus pinaster*. The inorganic part affects the plant combustion. Some mineral matter, present in the fuel, strongly catalyses the decomposition of cellulose components [20]. High ash contents decrease the volatilization rate, increase the residue and induce a lower temperature of active pyrolysis [1].

Table 1
Ultimate analysis of three fuels (wt. %)

Fuel	Elements			
	C	H	O	Ash
Pinus pinaster	50.64	6.76	41.53	1.07
Erica arborea	52.43	6.98	35.92	4.67
Cistus monspeliensis	46.58	6.22	37.68	9.52

3.2.2. Density

The mean densities of the samples are 927, 831 and 904 kg m^{-3} respectively for *Pinus pinaster*, *Erica arborea* and *Cistus monspeliensis*. These values are higher than for uncrushed plants [6]. Crushing exposes all the internal structure of leaves and thus involves the apparition of gaps in the mesophyll and conducting tissues. For a same mass, the volume of the crushed samples is lower than the uncrushed plants' ones increasing their density.

3.2.3. Surface-to-volume ratio

The mean surface-to-volume ratios of the samples are 6494, 6755 and 7198 m^{-1} respectively for *Pinus pinaster*, *Erica arborea* and *Cistus monspeliensis.* The surface-to-volume ratio of *Cistus monspeliensis* is higher than the two other's ones. In literature [21], the surface-to-volume ratios of the uncrushed plants are very different as they are around 4260 m^{-1} for *Pinus pinaster*, 8200 m^{-1} for *Erica arborea* and 3250 m^{-1} for *Cistus monspeliensis*. The crushing and the sieving allow obtaining samples with a comparable surface-to-volume ratio. The influence of this factor was thus minimized allowing us studying the impact of the other parameters.

3.2.4. Thermal diffusivity

3.2.4.1. Specific heat. The mean specific heats between 80 and 200 °C of the sample are 2017, 1856 and 1834 J kg^{-1} K^{-1} respectively for *Pinus pinaster*, *Erica arborea* and *Cistus mon-*

Table 2
Thermal conductivities for the three samples

Thermal conductivity ($W\,m^{-1}\,K^{-1}$)		
Species	Temperature (°C)	
	100	200
Pinus pinaster	0.112	0.119
Erica arborea	0.115	0.119
Cistus monspeliensis	0.107	0.115

speliensis. Some little fluctuations were observed during the measurements. They were due to two endothermic reactions:

- The vaporization of the water occurred around 100 °C. Water content (less than 2%) came from the self-rehydration of the fuel.
- The release of volatile organic compounds like terpenic molecules [22] that took place below the pyrolysis temperature [23].

However, the influence of these endothermic reactions can be neglected as, during this range of temperatures, the specific heat varies slightly around the mean value. The standard deviation is less than 5%. The specific heat of the three species is roughly the same. The specific heats of *Erica arborea* and *Cistus monspeliensis* are very close whereas the *Pinus pinaster* one is slightly higher. In literature, few data concerning vegetal fuel are reported apart from wood. The specific heat of dry wood depends on temperature and is given by [24]:

$$C_{p_{\text{drywood}}} = 103.1 + 3.867T \tag{6}$$

Thus, the specific heat of dry wood is 1545 and 1932 $J\,kg^{-1}\,K^{-1}$ respectively at 100 and 200 °C. These values are near our results.

3.2.4.2. Bulk density. The bulk densities of the crushed samples are 365, 376 and 298 $kg\,m^{-3}$ for *Pinus pinaster*, *Erica arborea* and *Cistus monspeliensis,* respectively. The mean standard deviation is less than 3.2%. The measurements are quite reproducible. According to the values of the density and to the bulk density, the fuel packing ratio is 39% for *Pinus pinaster*, 45% for *Erica arborea* and 33% for *Cistus monspeliensis.* In the experiments carried out at laboratory scale for fire across pine needles [11–14], the fuel packing ratio of the pine litters is about 3%.

3.2.4.3. Thermal conductivity. Table 2 shows the thermal conductivities of the samples at 100 and 200 °C. The standard deviation is 0.002. For the three fuels, the thermal conductivities are low (less than 0.2 $W\,m^{-1}\,K^{-1}$) and close. For the two temperatures, the thermal conductivity of *Erica arborea* is slightly higher than respectively *Pinus pinaster* and *Cistus monspeliensis*'s one. Between 100 and 200 °C, the change of thermal conductivity is essentially due to the vaporization of the water and the release of volatile organic compounds. At this extended range of temperature, no further change is observable for the thermal conductivities. Like for the specific heat, these two reactions can be neglected. While significant literature has been reported on thermal conductivity of wood, little has been reported on other vegetal fuel. The values obtained for wood are close to our results [25]. For the three samples, the thermal conductivity seems to be linked with the fuel packing ratio. For a same temperature, the sample with the highest fuel packing ratio exhibits the highest thermal conductivity. This tendency is reported by Suleiman et al. too [26].

Table 3
Thermal diffusivities for the samples

Thermal diffusivity ($m^2\,s^{-1}$)		
Species	Temperature (°C)	
	100	200
Pinus pinaster	1.52×10^{-7}	1.62×10^{-7}
Erica arborea	1.65×10^{-7}	1.71×10^{-7}
Cistus monspeliensis	1.96×10^{-7}	2.1×10^{-7}

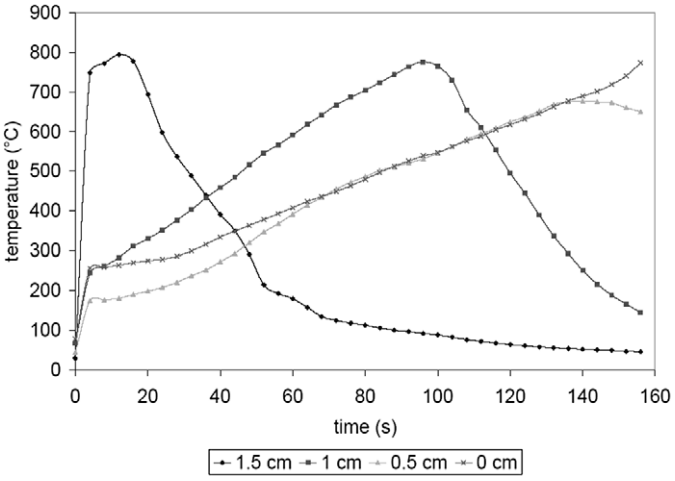

Fig. 5. Temperature of *Pinus pinaster* on the surface sample.

3.2.4.4. Thermal diffusivity. The thermal diffusivity (noted a) is given by the relation:

$$a = \frac{\lambda}{\rho_{\text{bulk}} \cdot C_p} \tag{7}$$

Table 3 presents the thermal diffusivities at 100 and 200 °C for the three samples. For both temperatures, the highest thermal diffusivity is obtained for *Cistus monspeliensis* followed by *Erica arborea* and *Pinus pinaster*.

3.2.5. Sample temperature

The sample temperature was determined by using the horizontal array of thermocouples located on the crushed sample (Fig. 1(b)). For the three fuels, the surface temperature follows the same trend. Fig. 5 shows only the mean surface temperature of *Pinus pinaster* for five experiments. Around 10 s, the maximum temperature is located at 1.5 cm, which corresponds to the position of the flame sheet. At this moment, the remaining part of the surface is heated by radiant heat flux leading to a linear temperature increase. After 20 s, the flame sheet moves towards the centre and the temperature decrease at 1.5 cm. At 80 s,

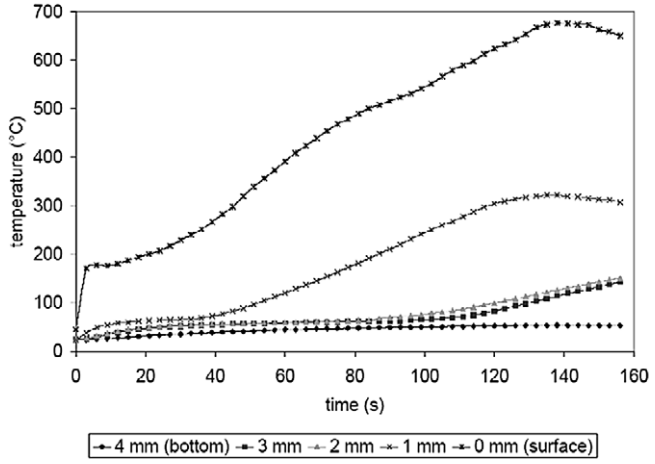

(a)

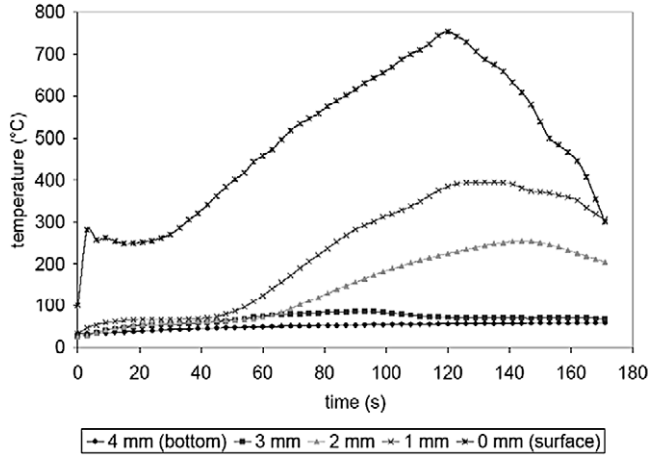

(b)

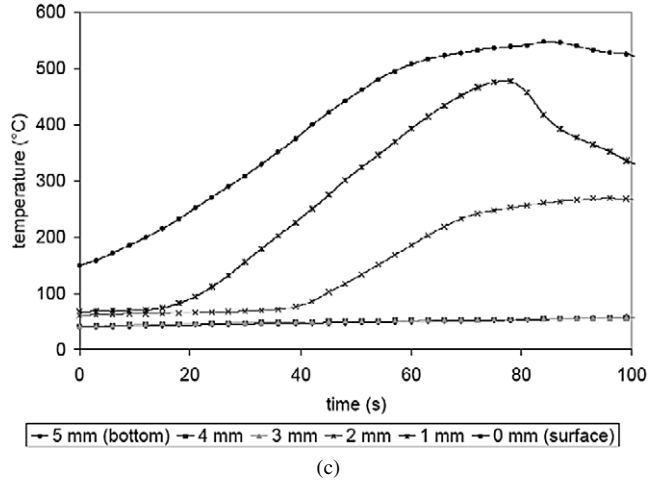

(c)

Fig. 6. Temperature along the depth of the sample at 5 mm from the centre for (a) *Pinus pinaster*, (b) *Erica arborea*, (c) *Cistus monspeliensis*.

the reaction zone of the flame arrives at 1 cm from the centre. We observe the same trend: the temperature reaches a maximum and then decreases with the radius reduction. Thus, the evolution of the surface temperature highlights the regression of the flame base during the burning.

Inside the sample, the temperature increases differently according to the fuel. Fig. 6 (a) to (c) shows the mean temperature along the depth of the sample at 5 mm from the centre for the three species. It is possible to observe a propagation of the heat wave in the sample. The particles are heated by conduction from the surface to the bottom. Below 200 °C, the sample does not degrade. Thus, for the whole fuels, near the support, the sample temperature is too weak so that the sample degrades. This observation explains the presence of the unburned fuel at this location (Fig. 4). For *Pinus pinaster*, only the particles located on the first millimetre under the surface give a sufficient temperature to degrade. For *Erica arborea* and for *Cistus monspeliensis,* the sample degrades over the two first millimetres. However, the temperature recorded at 1 mm under the surface is higher for *Cistus monspeliensis* than for *Erica arborea.* Thus, the heat diffusion is more significant in the sample depth for *Cistus monspeliensis* than respectively for *Erica arborea* and *Pinus pinaster.* This behavior is in agreement with the thermal diffusivities of the samples (Table 3) as the thermal diffusivity of *Cistus monspeliensis* is greater than *Erica arborea*'s and *Pinus pinaster*'s ones.

3.2.6. Mass loss

The load cell allowed obtaining the evolution of the mass loss for the three samples. The mean mass loss was calculated from five experiments and approximated by 4th order polynomials (Fig. 7(a)). The global mass loss of the samples is 0.14, 0.25 and 0.15 g respectively for *Pinus pinaster, Erica arborea* and *Cistus monspeliensis*. It corresponds to a percentage between 10 and 18% of the combustible part of the samples (sample mass minus ash proportion).

During the ignition stage, the most significant mass loss is observed for *Cistus monspeliensis* followed by *Erica arborea* and *Pinus pinaster*. The combustion of *Cistus monspeliensis* stops quickly in the laminar stage whereas the mass loss of the two other samples goes on. This difference of combustion dynamics is mainly due to the surface-to-volume ratio of *Cistus monspeliensis*'s particles. As said previously, a high surface-to-volume ratio involves a most efficient absorption of the radiative heating leading to a quickest combustion [6]. Thus, for *Cistus monspeliensis*, the crushing and sieving of the leaves was not sufficient to decrease the effect of the surface-to-volume ratio. This result shows the interest to crush and sieve the vegetative fuels to observe the impact of the other physical properties on their combustion. The change of surface-to-volume ratio between *Erica arborea* and *Pinus pinaster* is less substantial (around 4%). It cannot induce the mass loss difference of the two samples. Two secondary parameters, the ash content (Table 1) and the thermal diffusivity of the samples (Table 3) can explain this behavior. Firstly, the amount of mineral is four times higher for *Erica arborea* than for *Pinus pinaster* involving a lower pyrolysis temperature for *Erica arborea* than for *Pinus pinaster* [1]. Secondly, the thermal diffusivity of *Erica arborea* is higher than the one of *Pinus pinaster*, leading to a more significant heat diffusion in the sample of *Erica arborea* (Fig. 6). Thus, the combination of these two parameters entail to a more significant degradation of *Erica arborea* and to an higher mass loss of this sample during the ignition stage.

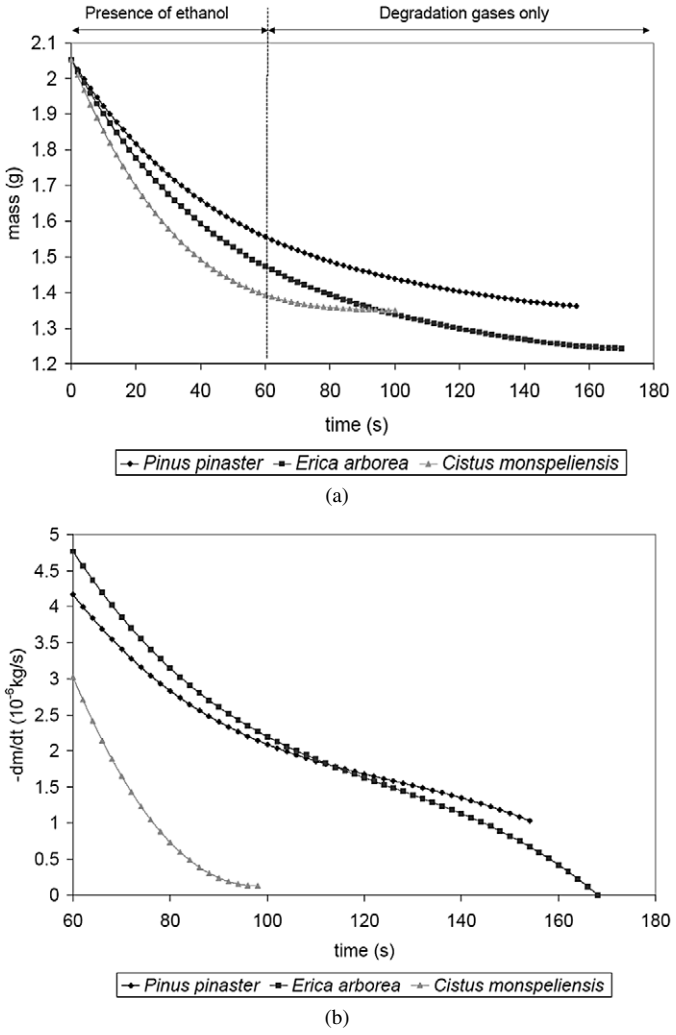

Fig. 7. (a) Mean mass loss for the three fuels. (b) Mean mass loss rate for the three fuels.

During the laminar phase, others factors control the mass loss of the samples. Fig. 7(b) presents the mean mass loss rate for the three fuels during this stage, approximated by 3rd order polynomials. The mass loss rates of *Cistus monspeliensis* are lower than the two other ones as this sample finishes its burning. Although the thermal degradation occurs deeper in the sample of *Erica arborea* (Fig. 6), the mass flow rate of degradation gases of *Erica arborea* and of *Pinus pinaster* are close. The degradation of *Erica arborea*'s sample produces more tar, which settles on the sample surface reducing the mass loss.

The mass loss is piloted by the value of the surface-to-volume ratio. However, for a same value it depends on the sample temperature, the ash content and the tar yield.

3.3. Description of the gas phase

3.3.1. Degradation gases

Table 4 shows the degradation gases analyzed for the three fuels. They consist of CO_2, CO, CH_4, H_2O, C_4H_6 and lower values of C_2 and C_4 hydrocarbons. These results are in agreement with the literature [15]. The degradation products released by *Pinus pinaster* contain more combustible gases than the other species (between 1.5 and 1.8 times more). The highest water content is observed for *Cistus monspeliensis.* The gases of *Erica arborea* hold more carbon dioxide than the two other fuels. All these gases come for the most part from the degradation of the ligno-cellulosic compounds. Hemicellulose degrades between 200 and 300 °C [27] and contributes weakly to the composition of degradation gases occurring during the range of temperature studied (280 to 430 °C). Cellulose is mainly responsible for the production of flammable volatile gases [28]. Between 300 and 350 °C, the formation of tar vapor from cellulose becomes predominant due to the decrease of its degree of polymerization. A deposit of tar on the reactor outside the furnace confirms this result. The degradation of lignin occurs between 225 and 450 °C. Although it produces some volatile gases, lignin is principally responsible for the char formation [29]. Thus, the degradation gases come mainly from cellulose [30].

Table 4
Mass fractions of the main pyrolysis gases released by the degradation of the three samples

Gas	Fuel		
	Pinus pinaster	*Erica arborea*	*Cistus monspeliensis*
CO	0.257	0.142	0.127
CO_2	0.494	0.722	0.590
CH_4	0.078	0.020	0.035
C_2H_4	0.010	0.004	0.007
C_2H_6	0.016	0.006	0.009
C_3H_6	0.001	0.001	0.004
C_3H_8	0.007	0.005	0.011
C_4H_6	0.034	0.040	0.051
C_4H_8	0.011	0.009	0.019
C_4H_{10}	0.003	0.003	0.008
H_2O	0.089	0.047	0.138
H_2	0.000	0.000	0.000
O_2	0.000	0.000	0.000

3.3.2. Radial temperature

As the radial temperatures follow the same trend for the three species, the mean radial temperatures at 1 cm high for *Erica arborea* is only presented (Fig. 8(a)). During the first 60 s, the curves fluctuate due to the ignition with ethanol, then, they become smooth during the laminar stage. The maxima correspond to the crossing of the thermocouples by the flame sheet. As the flame height and radius decrease, these maxima move to the centre of the samples. Fig. 8(b) shows the mean radial temperature at 1 cm high at 60, 110 and 160 s. As the flame comes through the array of thermocouples, the temperature distribution obtained on Fig. 8(b) is characteristic of the profile obtained for a diffusion flame [31].

3.3.3. Vertical temperature

Like for the radial temperature, the vertical temperatures follow the same trend for the three species. The mean time evolution of temperature for thermocouples number 1, 2, 3, 4, 5, 7 and 11 are presented in Fig. 9 for *Erica arborea*,

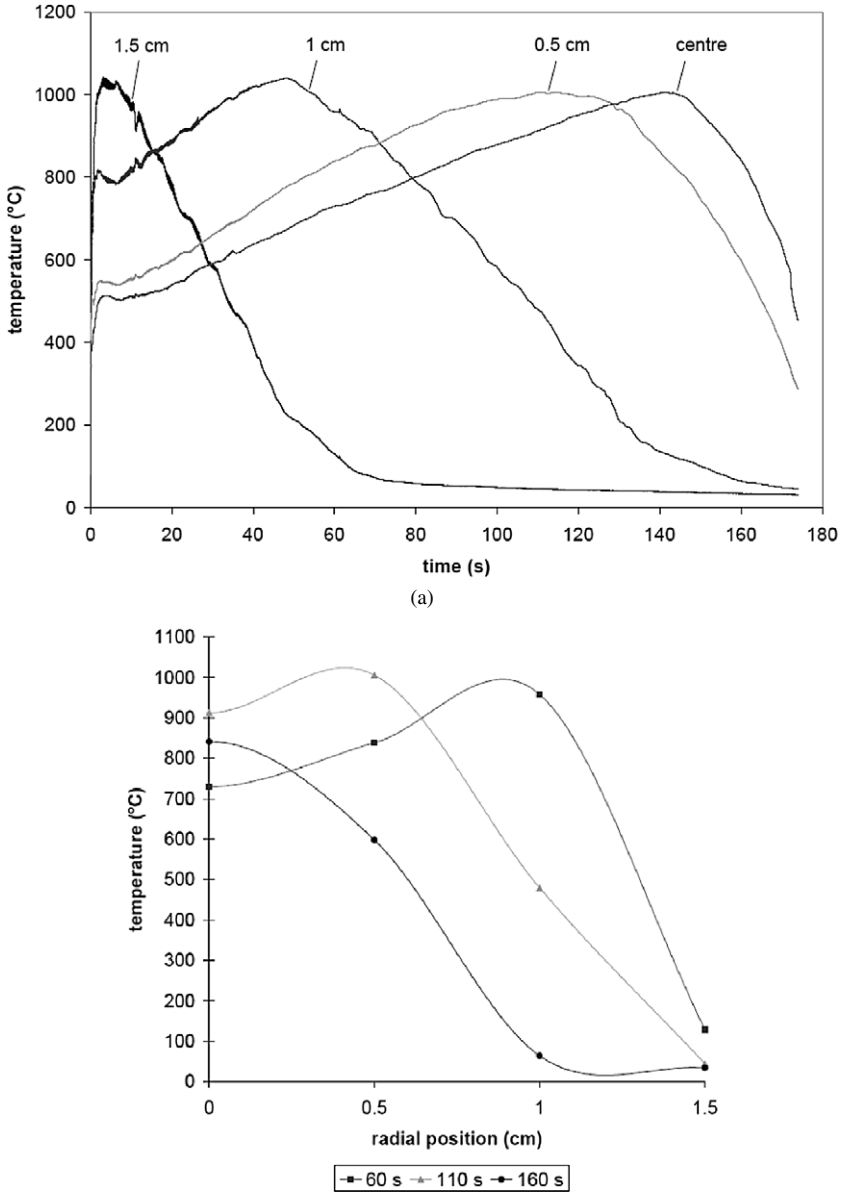

Fig. 8. Mean radial temperatures at 1 cm high for *Erica arborea* (a) versus time, (b) versus the radial temperature for different times.

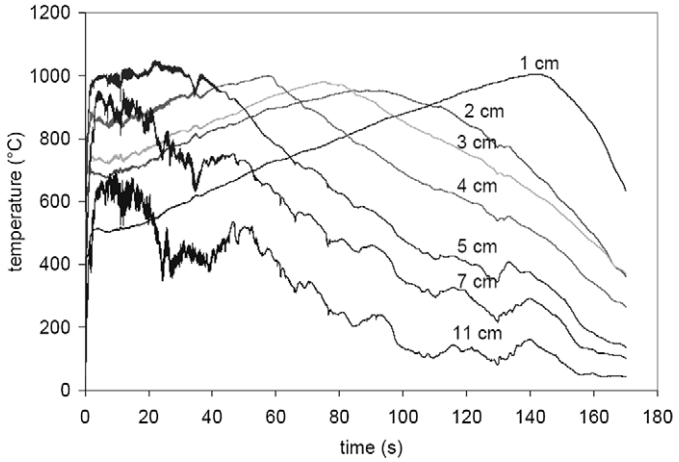

Fig. 9. Mean temperatures along the flame axis for *Erica arborea*.

as they are representative of the fire plume. The first stage of the flame (presence of alcohol) lasts approximately 60 s and will not be considered in the following. At the beginning of the second stage, thermocouples 1 to 5 take place inside the laminar flame, while the others (thermocouples 7 and 11) are located above it. The maximum temperature observed in the flame is around 1000 °C. As the flame decreases during this stage, thermocouples 1 to 3 remain wrapped up in the flame. Thermocouples 4 and 5 cross the flame during its regression recording successively the temperature of the flame and that of the thermal plume. The temperature decreases progressively from 800 °C to the ambient. The temperature recorded by the upper thermocouples (thermocouples 7 and 11) decrease slowly from 600 °C to the ambient with more fluctuations, since the flow becomes progressively turbulent in the thermal plume.

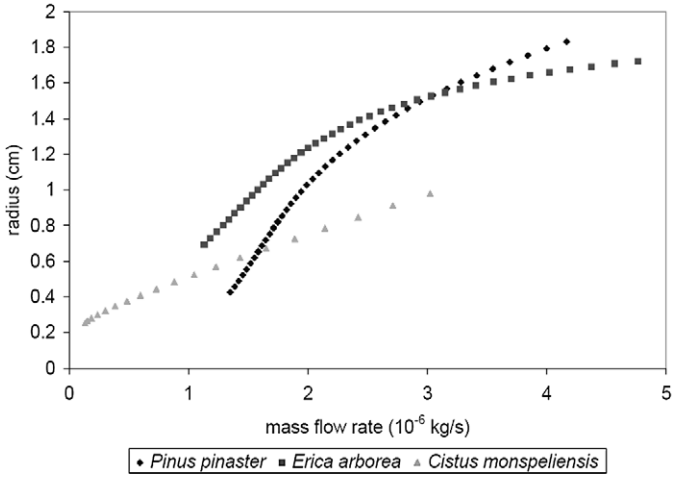

Fig. 10. Visible flame radius versus mass flow rate of degradation gases.

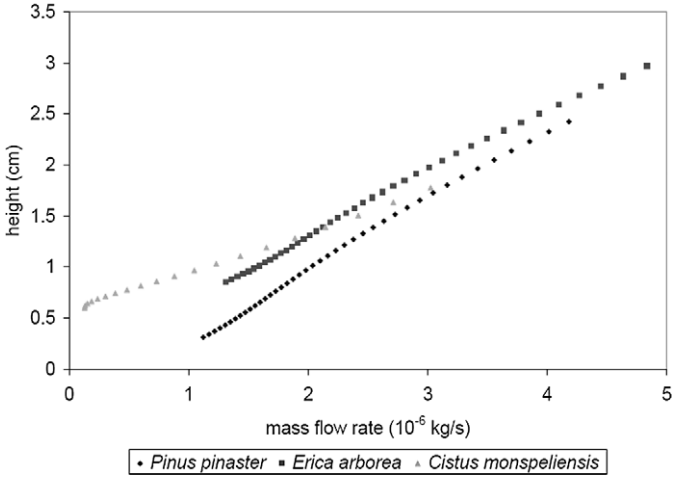

Fig. 11. Visible flame height versus mass flow rate of degradation gases.

3.4. Coupling between the sample and the flame

The coupling between the sample and the flame can be particularly highlighted by two variables: the flame geometry and the temperature distribution.

3.4.1. Flame geometry

The geometrical description of the flame was managed with two visible cameras (Fig. 1). Fig. 10 shows the visible radius of the flame base as a function of mass flow rate. The flame radius of *Cistus monspeliensis* decreases linearly with the mass flow rate. For the two other species, the radius decrease is slow for high mass flow rate. But, when the mass flow rate reduces, the regression of the flame base is more significant. For a given flow rate, the flame radius of *Cistus monspeliensis* is smaller than for the other species. It is certainly due to the high thermal diffusivity of this sample. Fig. 11 presents the visible flame height versus the mass flow rate of the degradation gases. These curves can be approximated by a straight line. For *Cistus monspeliensis*, the slope of the curve changes for heights lower than 0.5 cm. This part of the graph corresponds to the flame extinction. Contrary to the two other species, the flame extinction of

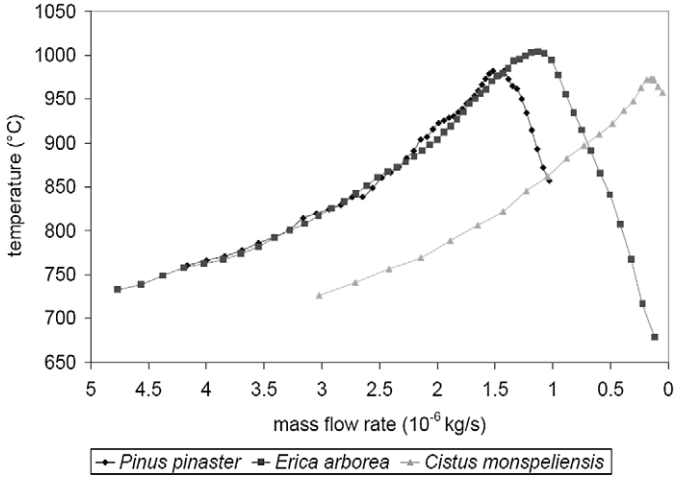

Fig. 12. Mean temperature along the flame axis and at 1 cm high versus the mass flow rate of the degradation gases.

Cistus monspeliensis is gradual. According to Fig. 11, the flame height and the mass flow rate of the degradation gases are also proportional. This behavior of laminar flame was also depicted by Jost [32]. The highest coefficient of proportionality is obtained for *Pinus pinaster* followed by *Erica arborea* and *Cistus monspeliensis*.

In order to study the influence of the degradation gases on the flame geometry, we compared the flame height of *Pinus pinaster* and *Erica arborea* for the same mass flow rate (around 3×10^{-6} kg s^{-1}) and flame radius (1.5 cm in Fig. 10). We can see in Fig. 11 that the flame height is taller for *Erica arborea* than for *Pinus pinaster*. As the mass flow rates of the gases and the flame radiuses are identical, this difference can be only due to the degradation gases released by the fuels (Table 4).

3.4.2. Temperature distribution

Fig. 12 presents the mean temperature at 1 cm high versus the mass flow rate of the degradation gases. We reversed the abscissa axis to follow the chronology of the experiments (high mass flow rates correspond to the beginning of the laminar stage). The curves of *Erica arborea* and *Pinus pinaster* are close whereas *Cistus monspeliensis*'s one differs. In these graphs, we can distinguish three regions:

- For the highest mass flow rates (until 2, 1.5 and 0.5×10^{-6} kg s^{-1} respectively for *Pinus pinaster, Erica arborea* and *Cistus monspeliensis)*, the thermocouple at 1 cm high is in the fuel rich zone where an oxygen deficit appears. When the flow rate decreases, the flame approaches thermocouple and the temperature increases steadily. For a same flow rate, the gas temperature of *Cistus monspeliensis* is higher than *Erica arborea*'s one and *Pinus pinaster*'s one.
- For a mass flow rate of 2, 1.5 and 0.5×10^{-6} kg s^{-1} respectively for *Pinus pinaster, Erica arborea* and *Cistus monspeliensis*, the thermocouple hits the combustion zone. The mean temperature is maximal and is around 1000 °C for the three fuels. The heating value per mass of air is calculated from the composition of degradation gases (Table 4) thanks

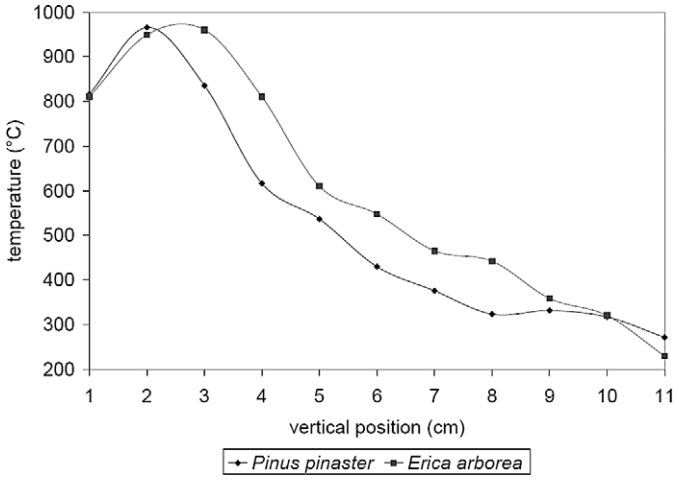

Fig. 13. Mean temperature along the flame axis versus the vertical position for *Pinus pinaster* and *Erica arborea* and for a mass flow rate equal to 3×10^{-6} kg s^{-1}.

to the following relation:

$$\Delta h_a = \Delta h f_s \tag{8}$$

where Δh is the reaction enthalpy of degradation gases (10.28, 5.61 and 8.01 MJ kg^{-1} respectively for *Pinus pinaster, Erica arborea* and *Cistus monspeliensis*) and where f_s corresponds to the stoechiometric coefficient in air (0.31, 0.59 and 0.40 respectively, for *Pinus pinaster, Erica arborea* and *Cistus monspeliensis*). The heating value per mass of air calculated for each gas composition is 3.23, 3.29 and 3.19 MJ kg$_{air}^{-1}$ respectively for *Pinus pinaster, Erica arborea* and *Cistus monspeliensis.* Although the reaction enthalpies of the degradation gases are very different, the heating values per mass of air are close for the three fuels as the reaction is piloted by the available dioxygen during the combustion. These values explain the weak differences of maximal temperature in flames.

- After the last range of mass flow rate, the temperature decreases as the thermocouple is up to the reaction zone, at the beginning of the thermal plume.

To study the influence of the degradation gases on the temperature, we compared its distribution along the flame axis for *Pinus pinaster* and *Erica arborea* for the same mass flow rate (around 3×10^{-6} kg s^{-1}) and same flame radius (1.5 cm in Fig. 10). Fig. 13 presents the mean axial temperature versus the vertical position for these fuels. The two curves give the same maximal temperature. However, the temperature profiles are different. The combustion of *Pinus pinaster* takes place closer to the surface sample than *Erica arborea*'s one. The combustion kinetics is also different and depends on the composition of degradation gases. In the thermal plume, the temperature decrease is identical for the two species. The temperatures are controlled by the radiation losses in the lower part and by the mixing of burnt gases with air in the upper part.

Thus, the temperature distribution recorded by the thermocouples is linked to the mass flow rate. Although the maximal temperatures are close for the whole species, their combustion kinetics varies following the composition of their degradation gases.

4. Conclusions

Surface-to-volume ratio is the driving parameter of forest fuel combustion. To understand the influence of the other parameters, the burning of crushed vegetative fuels was studied. This influence can be described as follows:

The sample mass loss depends on:

- The surface-to-volume ratio. We decreased its influence by crushing the samples.
- The temperature of the whole sample, which depends on the thermal diffusivity.
- The ash content of the plants and the tar production.

In the gas phase:

- Six main gases were identified during the thermal degradation of fuels: CO, CH_4, CO_2, H_2O and C_4H_6.
- The maximal temperature in the flames is roughly the same for the three species as the heating values per mass of air of their degradation gases are close.
- The temperature profiles vary among vegetative fuels in the flame as the combustion kinetics depends on the composition of degradation gases. The differences inside the thermal plume are less important because of the radiation losses and the mixing of burnt gases with air.

Concerning the coupling between the sample and the flame:

- The flame height is proportional to the mass flow rate.
- The flame height depends on the composition of the degradation gases.

Theses results obtained with laminar flames cannot be directly extended to real vegetation. However, this study can help to explain the combustion processes occurring in a larger scale more realistic fire. For laminar flames, the dynamics is influenced by the mass burning rate of the sample whereas the combustion kinetics depends on the degradation gas composition. By assuming that the chemistry of combustion remains the same as those associated to turbulent flames, the degradation gases should act upon them too. Thus, to improve the detailed models of forest fires [33,34], the degradation gases should be taken into account more precisely in particular by incorporating the main pyrolysis gases. With this in mind, the gas composition provided in this work can be used for the implementation of such models instead of the Grishin's hypothesis [15]. To go further into the improvement of forest fire modeling, we will test Grishin's hypothesis and investigate gas phase combustion mechanisms which consider the main degradation gases released by the vegetative fuels.

Appendix A

To increase the precision of specific heat measurement, an original method was applied in this study. The mean specific heat was calculated from its definition:

$$mC_p = \left(\frac{\partial h}{\partial T}\right)_P \tag{A.1}$$

where the sample mass m is constant.

The integration of Eq. (A.1) between T_k and T_{k+1} gives:

$$m\int_{T_k}^{T_{k+1}} C_p\,dT = \int_{T_k}^{T_{k+1}} \left(\frac{\partial h}{\partial t}\right)_P \left(\frac{\partial t}{\partial T}\right)_P dT = \frac{1}{\beta}\int_{T_k}^{T_{k+1}} HF\,dT \tag{A.2}$$

where β is the heating rate and HF stands for the heat flow.

The left-hand side of Eq. (A.2) was estimated as follow:

$$\int_{T_k}^{T_{k+1}} C_p\,dT = C_{p,\mathrm{mean}}(T_{k+1} - T_k) \tag{A.3}$$

where $C_{p,\mathrm{mean}}$ is the mean value of C_p on the interval $[T_k, T_{k+1}]$.

The fuel sample was placed in an aluminium pan. The DSC measures the heat flows (HF) of the sample and that of an empty pan. The heat flow released by the fuel sample is given by:

$$HF_{\mathrm{sample}} = HF_{\mathrm{measured}} - HF_{\mathrm{empty}} \tag{A.4}$$

Finally, for the sample and the reference (i.e., zinc), Eq. (A.2) becomes:

$$m_{\mathrm{sample}} C_{p_{\mathrm{mean,sample}}}(T_{k+1} - T_k) = \frac{1}{\beta}\left(\int_{T_k}^{T_{k+1}} HF_{\mathrm{sample}}\,dT - \int_{T_k}^{T_{k+1}} HF_{\mathrm{empty}}\,dT\right) \tag{A.5}$$

$$m_{\mathrm{reference}} C_{p_{\mathrm{mean,reference}}}(T_{k+1} - T_k) = \frac{1}{\beta}\left(\int_{T_k}^{T_{k+1}} HF_{\mathrm{reference}}\,dT - \int_{T_k}^{T_{k+1}} HF_{\mathrm{empty}}\,dT\right) \tag{A.6}$$

By dividing Eq. (A.5) by Eq. (A.6), the mean value of $C_{P_{\mathrm{mean,sample}}}$ on the interval $[T_k, T_{k+1}]$ is:

$$C_{p_{\mathrm{mean,sample}}}(T_{k+1} \to T_k) = C_{p_{\mathrm{mean,reference}}}\frac{m_{\mathrm{reference}}}{m_{\mathrm{sample}}} \times \frac{\int_{T_k}^{T_{k+1}} HF_{\mathrm{sample}}\,dT - \int_{T_k}^{T_{k+1}} HF_{\mathrm{empty}}\,dT}{\int_{T_k}^{T_{k+1}} HF_{\mathrm{reference}}\,dT - \int_{T_k}^{T_{k+1}} HF_{\mathrm{empty}}\,dT} \tag{A.7}$$

The determination of $C_{p_{\mathrm{mean,sample}}}(T_{k+1} \to T_k)$ implies the knowledge of $C_{p_{\mathrm{mean,reference}}}$. According to [35], the specific heat of zinc is given by:

$$C_{p_{\mathrm{reference}}} = 362.5 + 5.25 \times 10^{-2} T + 1.16 \times 10^{-4} T^2 \tag{A.8}$$

The integration of Eq. (A.8) on interval $[T_k, T_{k+1}]$ provides:

$$\int_{T_k}^{T_{k+1}} C_{p_{\mathrm{reference}}}\,dT = (T_{k+1} - T_k)\left[362.5 + \frac{5.25 \times 10^{-2}}{2}(T_k + T_{k+1}) + \frac{1.16 \times 10^{-4}}{3}\left(T_k^2 + T_k T_{k+1} + T_{k+1}^2\right)\right] \tag{A.9}$$

By identification with Eq. (A.3), we obtain for $C_{p_{\mathrm{mean,reference}}}$:

$$C_{p_{\mathrm{mean,reference}}} = 362.5 + \frac{5.25 \times 10^{-2}}{2}(T_k + T_{k+1}) + \frac{1.16 \times 10^{-4}}{3}\left(T_k^2 + T_k T_{k+1} + T_{k+1}^2\right) \tag{A.10}$$

References

[1] C.W. Philpot, Influence of mineral content on the pyrolysis of plant materials, Forest Science 16 (1970) 461–471.

[2] P. Ghetti, L. Ricca, L. Angelini, Thermal analysis of biomass and corresponding pyrolysis products, Fuel 5 (1996) 565–573.

[3] A.P. Dimitrakopoulos, Thermogravimetric analysis of Mediterranean plant species, J. Anal. Appl. Pyrolysis 60 (2001) 123–130.

[4] V. Leroy, D. Cancellieri, E. Leoni, Thermal degradation of lingo-cellulosic fuels: DSC and TGA studies, Thermochim. Acta 451 (2006) 131–136.

[5] W. Klose, S. Damm, W. Wiest, Pyrolysis and Activation of Different Woods–Thermal Analysis (TG/EGA) and Formal Kinetics, Proc. Int. Symp. of Catal. and Thermochem. Conv. of Nat. Org. Polym. 4 (2000) 9–17.

[6] J.L. Dupuy, J. Maréchal, D. Morvan, Fires from cylindrical forest fuel burner: Combustion dynamics and flame properties, Combust. Flame 135 (2003) 65–76.

[7] M. Saâdaoui, N. Mahjoub Saïd, H. Mhiri, Ph. Caminat, G. Le Palec, Ph. Bournot, Study of the behaviour of a flame resulting from the combustion of pine needles in a cylindrical basket, Int. J. Therm. Sci. 47 (2008) 293–305.

[8] R.C. Rothermel, H.E. Anderson, Fire spread characteristics determined in the laboratory, USDA For. Serv. Res. Pap. INT-30, Ogden, Utah, 1966.

[9] H.E. Anderson, Predicting wind-driven wild land fire size and shape, USDA For. Serv. Res. Pap. GTR-INT-305, 1983.

[10] D.X. Viegas, Convective processes in forest fires, in: Proc. NATO Adv. Study Institute on Buoyant Convective in Geophysical Flows, Kluwer, 1998, pp. 401–420.

[11] J.L. Dupuy, Slope and fuel load effects on fire behaviour: Laboratory experiments in pine needless fuel beds, Int. J. Wildland Fire 5 (1995) 153–164.

[12] W.R. Catchpole, E.A. Catchpole, R.C. Rothermel, G.A. Morris, B.W. Butler, D.J. Latham, Rate of spread of free-burning fires in woody fuels in a wind tunnel, Comb. Sci. Tech. 131 (1998) 1–37.

[13] J.M.C. Mendes-Lopes, J.M.P. Ventura, J.M.P. Amaral, Flame characteristics, temperature-time curves and rate of spread in fires propagating in a bed of *Pinus pinaster* needles, Int. J. Wildland Fire 12 (2003) 67–84.

[14] T. Marcelli, P.A. Santoni, A. Simeoni, E. Leoni, B. Porterie, Fire spread across pine needle fuel beds: Characterization of temperature and velocity distributions within the fire plume, Int. J. Wildland Fire 13 (2004) 37–48.

[15] A.M. Grishin, A.D. Gruzin, V.G. Zverev, Study of the structure and limits of propagation of the front of an upstream forest fire, Fizika Goreniya i Vzryva 21 (1985) 11–21.

[16] R.K. Mohammed, A. Tanoff, M.D. Smooke, A.M. Schaffer, M.B. Long, Computational and experimental study of a forced, time-varying, axisymmetric, laminar diffusion flame, Proc. Combust. Inst. 27 (1998) 693–702.

[17] R.C. Gonzales, R.E. Woods, S.L. Eddins, Digital Image Processing Using Matlab, Pearson Prentice Hall, 2004.

[18] S.E. Gustafsson, Transient plane source techniques for thermal conductivity and thermal diffusivity measurements of solid materials, Rev. Sci. Instrum. 62 (1991) 797–804.

[19] M.J. Safi, I.M. Mishra, B. Prasad, Global degradation kinetics of pine needles in air, Thermochim. Acta 412 (2004) 155–162.
[20] G. Várhegyi, J.A. Antal Jr., E. Jakab, S. Piroska, Kinetic modelling of biomass pyrolysis, J. Anal. Appl. Pyrolysis 42 (1997) 73–87.
[21] M. Cohen, P. Cuinas, C. Diez, P. Fernandes, M. Guijarro, C. Moro, FIRE STAR: A decision support system for fuel management and fire hazard reduction in Mediterranean wildland—urban interface. Wildland fuel particles characterisation: Database Content. D6-03 Annexe 1, 2003.
[22] S. Owen, C. Boissard, C.N. Hewitt, Volatile organic compounds (vocs) emitted from 40 Mediterranean plant species: Voc speciation and extrapolation to habitat scale, Atmos. Environ. 35 (2001) 5393–5409.
[23] V.A. Isidorov, V.T. Vinogorova, K. Rafalowski, HS-SPME analysis of volatile organic compounds of coniferous needle litter, Atmos. Environ. 37 (2003) 4645–4650.
[24] K.W. Ragland, D.J. Aerts, A.J. Baker, Properties of wood for combustion analysis, Bioresour. Technol. 37 (1991) 161–168.
[25] M. Gupta, T. Yang, C. Roy, Specific heat and thermal conductivity of softwood bark and softwood char particles, Fuel 82 (2003) 919–927.
[26] B.M. Suleiman, J. Larfeldt, B. Leckner, M. Gustavsson, Thermal conductivity and diffusivity of wood, Wood Sci. Technol. 33 (1999) 465–473.
[27] R.H. White, M.A. Dietenberger, Wood products: Thermal degradation and fire, in: Encyclop. of Mat. Sci. and Technol., 2001, pp. 9712–9716.
[28] S.L. LeVan, Thermal degradation, in: Concise Encyclopedia of Wood and Woodbased Materials, Pergamon, New York, 1989.
[29] J.J.M. Orfão, F.J.A. Antunes, J.L. Figueiredo, Pyrolysis kinetics of lignocellulosic materials—three independent reactions model, Fuel 78 (1999) 349–358.
[30] R. Alén, E. Kuoppala, P. Oesch, Formation of the main degradation compound groups from wood and its components during pyrolysis, J. Anal. Appl. Pyrolysis 36 (1996) 137–148.
[31] F.A. Williams, Combustion Theory, Addison-Wesley Publishing Company, Redwood City, 1985.
[32] W. Jost, Explosion and Combustion Processes in Gases, McGraw-Hill, 1946.
[33] O. Séro-Guillaume, J. Margerit, Modelling forest fires. Part I: A complete set of equations derived by extended irreversible thermodynamics, Int. J. Heat Mass Transfer 45 (2002) 1705–1722.
[34] D. Morvan, J.L. Dupuy, Modeling the propagation of a wildfire through a Mediterranean shrub using a multiphase formulation, Combust. Flame 138 (2004) 199–210.
[35] F. Massard, Aide-Mémoire du thermicien, Elsevier, 1997.